JPRS-CST-91-008
3 APRIL 1991

JPRS Report

Science & Technology

China

Radar Cross Section Studies

REPRODUCED BY
U.S. DEPARTMENT OF COMMERCE
NATIONAL TECHNICAL INFORMATION SERVICE
SPRINGFIELD, VA. 22161

Science & Technology

China

Radar Cross Section Studies

JPRS-CST-91-008 *3 April 1991*

CONTENTS

Scattering Mechanism, RCS Reduction of Antennas

91FE0324A Beijing YUHANG XUEBAO [JOURNAL OF CHINESE SOCIETY OF ASTRONAUTICS] in Chinese No 4, Oct 90 pp 94-99 [MS received 23 Feb 89]

[Article by Ruan Yingzheng [7086 4481 6927] of the University of Electronic Science and Technology of China, Chengdu, project funded by the Institute of Electronics and Nanchang Aircraft Corporation: "Scattering Mechanism and Reduction of Radar Cross Section of Antennas"]

[Text] **Abstract**

A strong scattering source in the nose-cone direction of a flying vehicle is its antenna. Its contribution to the radar cross section (RCS) includes the structural-scattering term and the mode-scattering term caused by retransmission. The latter is unique to an antenna which is a loaded scatterer. This paper presents the scattering mechanism and analytical computation method for these two terms and introduces several technical ways to reduce RCS and their effectiveness.

I. Introduction

In order to improve the survival and penetration capability of modern military aircraft, it is necessary to minimize the effective RCS of the target. Results from a great deal of experimental work show that an antenna is a very strong scattering source from certain viewing angles. For example, the paraboloidal antenna at the front contributes significantly to the RCS in the nose-cone direction. Since an antenna is an energy transducer between free waves and guided waves, it has excellent electrical properties during reception in order to provide maximum signal power to the load (receiver). Therefore, the scattering from a receiving antenna is far more complex than that from an ordinary scattering body. In addition to the electromagnetic scattering generated by induced current on the antenna, reflected power due to load mismatch also results in a secondary current distribution on the antenna. Subsequently, the antenna retransmits. In order to effectively control and minimize RCS and not to affect its operation, it is necessary to study the scattering mechanism of antennas and analytical methods to calculate RCS in order to find feasible means to lower antenna RCS.

II. Scattering Mechanism of Antennas

Foreign scholars performed theoretical studies on antenna scattering as early as the 1950's-60's.[1-7] They treated the transmitting antenna (T) which generates the incident electromagnetic wave, the scattering antenna (S) which passively scatters and retransmits electromagnetic wave and the receiving antenna (R) which detects the scattering field as a linear system with three terminals (see Figure 1). Various expressions for the scattering field [vector]E_s at the receiving antenna R were derived from network analysis. They all include two parts. First is a structural scattering term which is independent of the load of the scattering antenna. It is the scattering field generated by current induced on the antenna from the incident wave and is similar in mechanism to a normal scattering object. The other part is the antenna mode which varies with the load. It is the scattering field retransmitted by the antenna which is generated by reflected power due to load mismatch. This is unique for antennas because they are loaded scattering objects. Green[7] derived the following expression for such a scattering field with the physical significance discussed above:

$$\vec{E}_s(Z_l) = \vec{E}_s(Z_a^*) - \Gamma I(Z_a^*)\vec{E}_{s0} \qquad (1)$$

where [vector]$E_s(Z_l)$ is the scattering field of a scattering antenna under a load Z_l at receiving antenna R, [vector]$E_s(Z_a^*)$ represents the scattering field of the scattering antenna under conjugate matching load, Z_a^*, [vector]E_{so} is the field generated by a unit of exciting current at R, $I(Z_a^*)$ is the current generated by the scattering antenna from incident-wave excitation under conjugate matching load, and Γ is the voltage reflection coefficient due to load mismatch and can be expressed by the following equation:

$$\Gamma = (Z_l - Z_a^*)/(Z_l + Z_a) \qquad (2)$$

where Z_a is the impedance of the scattering antenna.

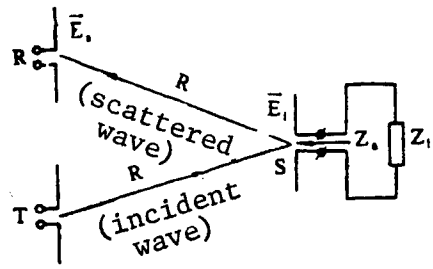

Figure 1. A Triple-Port System Consisting of Transmitting, Scattering, and Receiving Antennas

Obviously, the second term on the right hand side of equation (1) is the mode term and is dependent on the radiation characteristics of the antenna. Its scattering directivity diagram is the radiation directivity diagram of the antenna. Its corresponding RCS contribution is determined by the magnitude of the reflected wave. Hence, it is also known as the effective echo area.[6]

III. Analysis of Antenna RCS

The theoretical definition of RCS[8] (see Figure 1) is:

$$\sigma = \lim_{R\to\infty} 4\pi R^2 \frac{|E_s|^2}{|E_i|^2} \qquad (3)$$

were E_s includes both scattering fields shown in equation (1). The first term determines the structural RCS of the

antenna σ_s and the second term is the RCS from the antenna mode σ_e. The superposition of their phases is the overall RCS of the antenna:

$$\sigma = |\sqrt{\sigma_s} + \sqrt{\sigma_e} e^{j\psi}|^2 \qquad (4)$$

where ψ is the relative phase difference of the two scattering fields shown on the right hand side of equation (1). Usually, it is very difficult to analytically determine the structural term σ_s, mode term σ_e and phase difference ψ. It requires solving an extremely complicated electromagnetic-field boundary-value problem. In engineering, it is usually estimated using a variety of approximation methods.

In order to analyze the contribution of the mode term σ_e, let us refer to the three-antenna system shown in Figure 1. Assuming that the distance between the transmitting antenna and scattering antenna and that between the scattering antenna and receiving antenna are both equal to R and the gain function (directivity) of the scattering antenna is $G(\theta, \varphi)$, when the incident wave field is E_i, the amount of incident power captured by the scattering antenna is:

$$P_i = (E_i^2/120\,\pi)\, S_e(\theta_t, \varphi_t)\, \mu_t \qquad (5)$$

where $0 \leq \mu_t \leq 1$ is the polarization-matching factor between the transmitting antenna and scattering antenna. When polarization is completely in sync, $\mu_t = 1$. When they are orthogonal to each other, $\mu_t = 0$. $S_e(\theta_t, \varphi_t)$ is the effective reception area of the scattering antenna in the direction of the transmitting antenna (i.e., incident wave direction θ_t, φ_t). It can be determined by the gain factor of the antenna in that direction:

$$S_e(\theta_t, \varphi_t) = (\lambda^2/4\,\pi)\, G(\theta_t, \varphi_t) \qquad (6)$$

When there is load mismatch at the scattering antenna (Z_l not equal to Z_a^*), the power reflected is $P_i\Gamma^2$ and Γ is the voltage reflection coefficient which is determined by equation (2). This part of power is retransmitted by the antenna which produces the mode-scattering-field term E_s at the receiving antenna R. Its power density is:

$$E_s^2/120\,\pi = (P_i\Gamma^2/4\pi R^2)\, G(\theta_4, \varphi_r)\mu_r \qquad (7)$$

where $0 \leq \mu_r \leq 1$ is the polarization-matching factor between the scattering antenna and receiving antenna. $G(\theta_r, \varphi_r)$ is the gain factor in the direction of the receiving antenna (i.e., direction of scattering wave θ_r, φ_r).

By substituting equations (5), (6) and (7) into (2), it is possible to determine the contribution of the mode term to the RCS due to antenna retransmission.

$$\sigma_e = (\lambda^2/4\pi)\, (\theta_t, \varphi_r) G(\theta_r, \varphi_r)\, \mu_t\mu_r\Gamma^2 \qquad (8)$$

The above RCS equation is for two radar stations. For a single station (i.e., backscattering), because $G(\theta_t, \varphi_t) = G(\theta_r, \varphi_r) = G$, $\mu_t = \mu_r = \mu$. Hence, equation (8) is simplified to:

$$\sigma_e = (\lambda^2/4\pi)\, G^2\mu^2\Gamma^2 = S_eG\mu^2\Gamma^2 \qquad (9)$$

This equation indicates that with matching antenna polarization ($\mu = 1$) and total load reflection ($\Gamma = 1$), the mode term of RCS is equal to the product of effective reception area and gain:

$$\sigma_e = (\lambda^2/4\pi)\, G^2 = S_eG \qquad (10)$$

The structural term of RCS is dependent upon the type and structure of the antenna. Since its scattering mechanism is similar to an ordinary scattering body, σ_s can be calculated by conventional electromagnetic-wave scattering theory. When the size of the antenna is far greater than the radar wavelength, various high-frequency approximation methods, such as the geometric optics method, physical optics method, geometric diffraction method, and complex-ray method, are often used.[8-10] Figure 2 shows the structural term of the RCS (solid line)[11] in the X band of a Cassegrain antenna with primary and secondary diameter of 27 cm and 6.8 cm, respectively, using the geometric diffraction method and complex-ray method. When the secondary surface is replaced by a planar disk of identical diameter, the structural term σ_s is shown as the broken curve.[12] This demonstrates that antenna structure has a significant impact on σ_s.

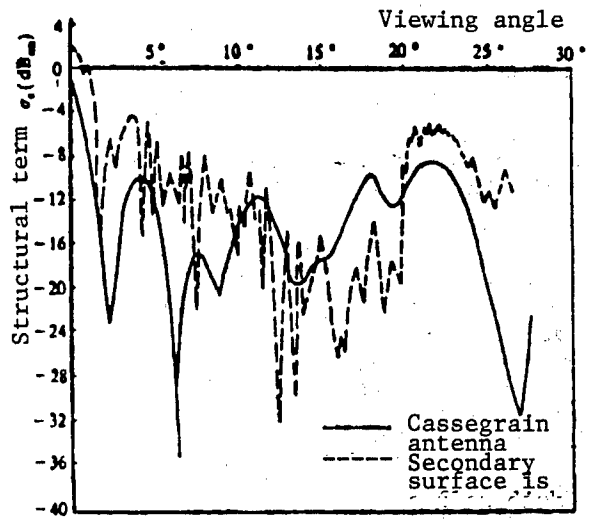

Figure 2. Calculated Structural Term of RCS of a Cassegrain Antenna (λ = 3.2 cm)

The phase difference ψ between the mode term and structure term of the scattering field is very difficult to model and calculate. It may be between zero and 2π. Therefore, total RCS given by (4) varies over a range:

$$\sigma_{min} = |\sqrt{\sigma_s} - \sqrt{\sigma_e}|^2 \leq \sigma \leq |\sqrt{\sigma_s} + \sqrt{\sigma_e}|^2 = \sigma_{max} \qquad (11)$$

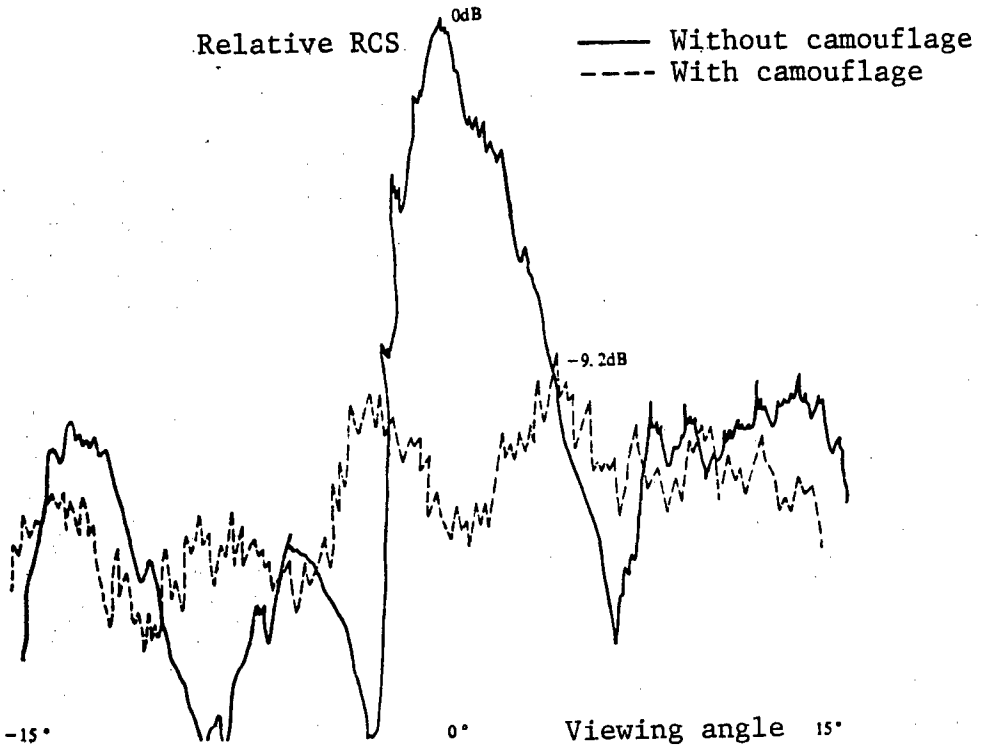

Figure 3. Experimental Results of Antenna Camouflage Technique

Usually, in order to estimate the RCS of an antenna, σ_s and σ_e are considered to be similar in magnitude and $\psi = 0$. Therefore, the total RCS of an antenna is:

$$\sigma \approx (\lambda^2/\pi)\, G^2 = 16\, \pi \nu^2\, (S_a/\lambda)^2 \qquad (12)$$

where G is the gain of the antenna, S_a is the geometric area of the antenna aperture, and ν is antenna aperture utilization coefficient. This equation shows that for a given antenna, the higher the radar frequency is the larger the RCS becomes. Using the 27-cm-diameter antenna shown in Figure 2 as an example, assuming $\nu = 0.25$, the RCS is $\sigma = 10$ dBsm [decibels per square meter] at $\lambda = 3.2$ cm. At $\lambda = 2$ cm, $\sigma = 14$ dBsm. Equation (12) is also applicable to linear antennas. For a shorted half-wave dipole antenna, $G \approx 1.64$, and therefore equation (12) yields $\sigma \approx 0.85\lambda^2$, which is in excellent agreement with experimental results.

IV. RCS Reduction Techniques

Usually, RCS can be reduced by shaping, using wave-absorbing materials and loading.[8] The RCS of an antenna, which is a loaded scattering body in a special shape, can be reduced as follows.

1. Low-RCS Profile Shield

This method employs a low-RCS profile shield to cover the antenna so that the incident radar wave is scattered by the shield, instead of entering the antenna, to lower its RCS. When the antenna is not in use (such as when a terminal-guidance radar or an airborne radar is not turned on), a metal shield can be used to "camouflage" the antenna; this is known as the antenna camouflage technique. Figure 3 shows the experimental results of the RCS of a 27-cm-diameter Cassegrain antenna before and after camouflage.[12] It shows that the RCS in the nose-cone direction could be lowered by approximately 10 dB. There are other types of antenna camouflage techniques such as "burying" the antenna into the fuselage, or rotating the antenna 90° and returning it to its normal position when in use. However, this requires sufficient space. It is structurally difficult to realize at the nose of a missile.

The above camouflage techniques cannot be used to reduce RCS when the antenna is in use. A filter type of shield may be used instead of a metal screen. It may be a high-pass, low-pass or band-pass filter, depending upon the operating frequency of the antenna and the frequency of the hostile radar (i.e., stealth frequency). The shield may be of a grid structure or an FSS (frequency selective surface) structure. Within the operating band of the antenna, the filter causes some insertion loss, but would not alter other characteristics of the antenna. With respect to other radar frequencies outside the antenna band, the filter shield has excellent reflection characteristics to prevent it from entering the antenna system. Using an inclined FSS flat plate, RCS can be reduced by approximately 10 dB.

2. Lowering RCS Within Antenna Operating Band

FSS shielding can only deal with RCS outside the operating band. It is ineffective within the operating band of the antenna. In order to lower RCS in the band, it is necessary to reduce the structure term and mode term of the scattering. To reduce the structure term, we have to use a low-RCS antenna system, such as the one we will discuss below. To reduce the mode term, it is necessary to match the load and polarization characteristics. From equation (9), with a given gain and frequency, the smaller the reflection coefficient Γ and polarization matching factor μ are, the smaller σ_e becomes. Figure 4 shows the dependence of σ_e upon Γ (or μ). It shows that if the voltage reflection coefficient $\Gamma = 0.1$ (corresponding to a voltage standing wave ratio of $\rho = 1.2$), then the mode term σ_e can be lowered by approximately 20 dB.

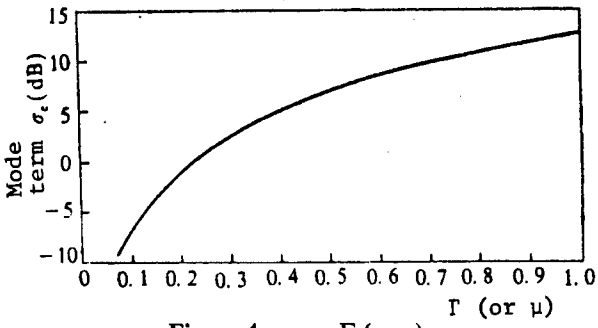

Figure 4. σ_e vs. Γ (or μ)

It is also possible to lower the RCS of the antenna with respect to an orthogonally polarized wave by using the polarization isolation property. If the antenna operates in a horizontally polarized mode, it is possible to use a vertical-grid low-RCS shield to reflect a vertically polarized wave in the band on the grid surface. A paraboloidal reflective surface may be made with a horizontal-grid structure to focus a horizontally polarized wave from the source reflected from the surface and to allow a vertically polarized incident radar wave to penetrate the surface and be absorbed by an absorbing material.

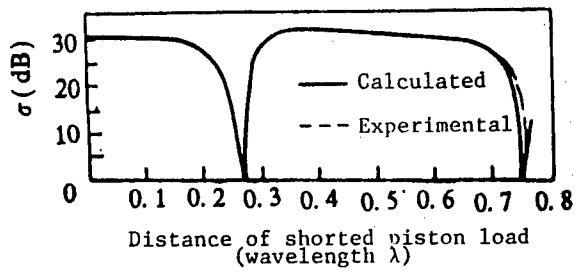

Figure 6. Effect of Load Position on RCS of Horn Antenna

3. Load-Cancellation Technique

From equations (4) and (11) we know that the phase difference ψ between the structure term and mode term has a significant impact on the total RCS. Although it is very difficult to theoretically analyze ψ, it can be adjusted by experimental means to make σ_s and σ_e cancel each other in order to reduce the total RCS. Figure 5 shows the monostatic RCS curves measured experimentally with a 27-cm-diameter Cassegrain antenna with a shorted piston added to the feeder.[12] Changing the position of the piston shifts the phase of the reflection coefficient (i.e., the mode term of the scattering field). The total RCS of the antenna can be reduced by approximately 10 dB. Figure 6 shows the effect of a pair of pistons on a horn antenna with G = 15.1 dB. Under optimal conditions, its RCS can be reduced by approximately 30 dB.[13]

In addition to adjusting ψ to cancel the two terms, it is also possible to introduce an artificial load. For instance, adding a load at the reflection surface of a Cassegrain antenna can lower its RCS by approximately 3-5 dB.[12]

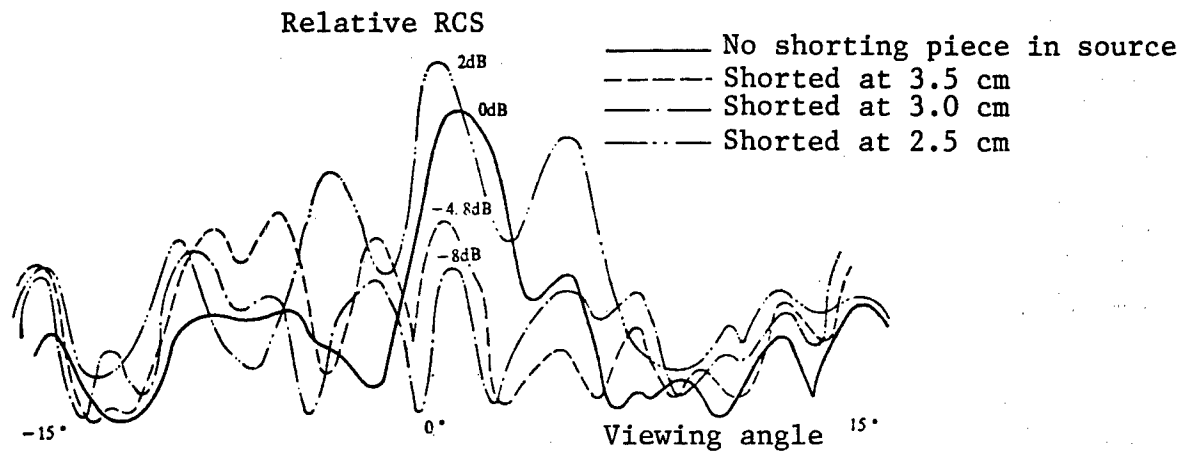

Figure 5. RCS of Cassegrain Antenna With Different Loads

The disadvantage of load cancellation is its frequency sensitivity. It can only be used in a narrow band. In order to deal with various radar frequencies, an adaptive loading technique must be used. Load amplitude and phase are adjusted on a real-time basis from detected parameters such as frequency, polarization and incident direction of the radar wave in order to reduce RCS in an optimal manner. Obviously, this would increase the complexity of the equipment tremendously.

4. Low-RCS Array Antenna Technique

Compared to an antenna with a reflective metallic surface, an array antenna system has better low-RCS characteristics. Because the structure-term RCS for a planar array antenna is proportional to the number elements, we should use high-gain low-RCS antenna elements, such as dielectric director elements or traveling wave microstrip elements, to the extent possible. In order to reduce RCS further, elements may be mounted on a suitable curved surface or directly installed on the surface of the flying object to form a "conformal" antenna array. In this case, simpler elements such as oscillator, slot, microstrip, etc., may be used. However, array design becomes very complicated. In order to obtain satisfactory antenna gain, side-lobe voltage, single-pulse sum-and-difference and beam-scanning characteristics, delicate calculations and adjustments are required. The number of antennas may be reduced by using phased-array multi-purpose antenna arrays to further lower the RCS of the target.

V. Conclusions

The study of RCS reduction of an antenna—as a strong scattering source of a flying object—has attracted attention all over the world. The preliminary discussion on antenna scattering mechanism and RCS reduction presented in this paper will aid this effort. Due to some unique characteristics of antennas, certain effective RCS-reduction methods (such as reshaping and wave-absorbing materials) cannot be directly applied to antennas. This makes stealth research on antennas very difficult. There is a great deal of theoretical and experimental work to be done in order to provide a satisfactory solution to this problem (not only lowering antenna RCS but also leaving its characteristics unaffected).

The author wishes to thank Han Xiaoying [7281 1420 5391], Feng Lin [7458 2651], Lei Ping [7191 1627], Lu Yilong [7120 0310 3478], Zhong Qingfeng [6988 1987 0023], and Deng Shuhui [6772 2579 6540] for their assistance in this work.

References

1. R. F. Harrington, "Electromagnetic Scattering by Antennas," IEEE TRANS., AP-11, 1963, pp 595-596.

2. R. F. Harrington, "Theory of Loaded Scatterers," PROC. IRE, Vol 111, 1964, pp 617-623.

3. J. K. Schindler, et al., "The Control of Electromagnetic Scattering by Impedance Loading," IEEE TRANS., AP-13, 1965, pp 993-1004.

4. Y. Y. Hu, "Back-Scattering Cross Section of a Center-Loaded Cylindrical Antenna," IRE TRANS., AP-6, 1958, p 140.

5. K. M. Chen, et al., "Minimization of Back Scattering of Cylinder by Central Loading," IEEE TRANS., AP-12, 1964, pp 576-582.

6. E. M. Kennaugh, "The Echoing Area of Antennas," Antenna Lab., Ohio State University, 1957, AD-152786.

7. R. B. Green, "The General Theory of Antenna Scattering," Antenna Lab., Ohio State University, Rep. No. 223-17, 1963.

8. E. F. Knott, et al., "Radar Cross Section" (translated by Ruan Yingzheng et al.), Electronics Industry Publishing House, 1988.

9. Ruan Yingzheng, "Using Complex-Ray Method in Stealth Technology," YINSHEN JISHU [STEALTH TECHNOLOGY], No 1, 1989, pp 18-27.

10. P. S. S. Kao, "Backscatter Cross Section of a Paraboloidal Antenna," Lincoln Lab., MIT, 1973, AD-770012.

11. Deng Shuhui and Ruan Yingzheng, "RCS of Reflective Antenna," PROC. ISAE 89, Shanghai, 1989.

12. Ruan Yingzheng and Feng Lin, "Study of Stealth Antennas and Radomes," Report No. 8489-4 of University of Electronic Science and Technology of China, Chengdu, 1988.

13. G. T. Ruck, et al., "Radar Cross Section Handbook," Vol 2, Chapter 8, Plenum Press, 1970.

Studies on Target Scattering and RCS

91FE0219A Beijing DIANZI XUEBAO [ACTA ELECTRONICA SINICA] in Chinese Vol 18 No 6, Nov 90 pp 92-96 [MS received Jul 89, revised Dec 89]

[Article by Ruan Yingzheng [7086 4481 6927] of the University of Electronic Science and Technology of China, Chengdu, project funded by the Institute of Electronics and Nanchang Aircraft Corporation: "Studies on Scattering and Radar Cross Section"]

[Text] **Abstract**

The scattering characteristics of military flying targets are described. High-frequency scattering mechanism, radar cross section (RCS) analysis methods, RCS reduction approaches and low-RCS target detection techniques are discussed. Some latest achievements and urgent problems are presented.

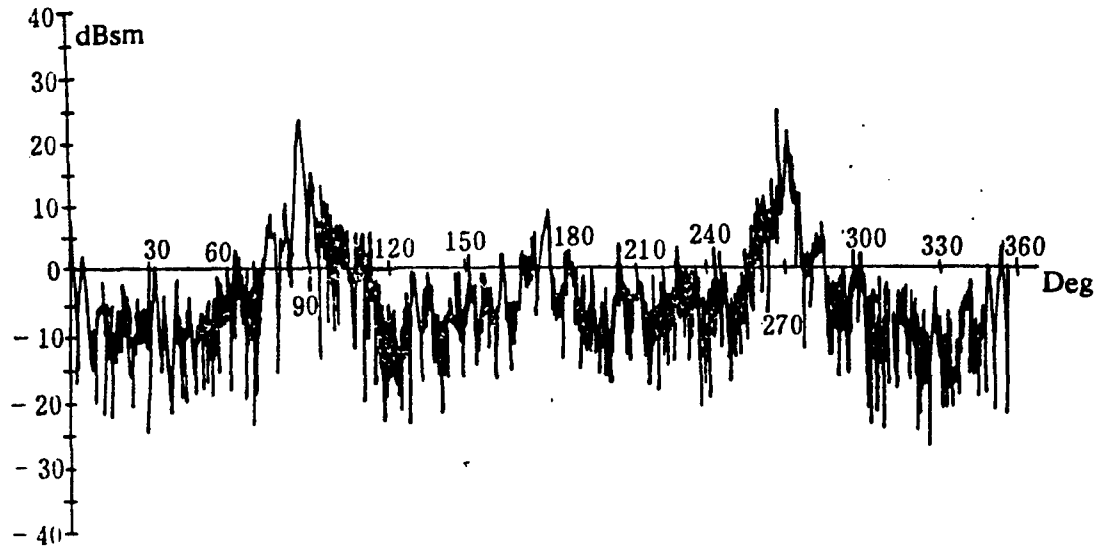

Figure 1. Measured RCS Directional Pattern of a Typical Target

I. Introduction

Since World War II, radar has been the most effective means of target detection. With leaping development in electronics and computer technology, radar performance continues to improve and its capabilities are constantly being perfected. It has become a fatal threat to any offensive weapons. To defeat radar and enhance the survivability and breakthrough capability of military targets, for over 20 years a number of powerful nations have been secretly conducting research on target scattering characteristics and stealth technology and have developed a variety of stealth airplanes and missiles.[1]

This paper describes the scattering mechanism of the electromagnetic wave of a radar from a target in flight, analysis methods and reduction techniques for RCS, and counter-stealth detection technology. The purpose is not to comprehensively present all existing theories and methods. Instead, it is focused on latest achievements and most urgent problems to be resolved.

II. High-Frequency Scattering Mechanism of Complex Target

The scattering of radar waves from a military target belongs to the domain of "high-frequency" scattering. Based on the local nature of a high-frequency field, the scattering of a complex target can be decomposed into several scattering centers. The total cross section is the sum of the RCS phases of all the individual scattering centers:[2,3]

$$\sigma = \left| \sum_{n=1}^{N} \sqrt{\sigma_n} \exp(j2k_t R_n) \right|^2 \qquad (1)$$

where σ_n and R_n represent the RCS of the nth scattering center and its distance to the threatening radar, respectively. When the target attitude angle varies, the above equation predicts an extremely large RCS fluctuation (target glimmer). Less than 1° change in attitude angle can lead to a 1-2 orders of magnitude of change in RCS. Figure 1 shows a measured RCS direction pattern of a typical missile model (X-band, horizontally polarized). It shows that the target has very strong echoes from lateral scattering and the nose cone.

The major mechanism of lateral scattering is mirror reflection from the target surface. Its scattering centers include the missile body, vertical tail and wings. They can be simulated by cone, plate and angle reflectors. Because the scattering mechanism is simple and easy to control, lateral scattering is not a major threat to the target.

The nose cone is a totally different story. The majority of threatening radar waves are in that area. Furthermore, there are numerous scattering centers in the nose-cone sector which are usually non-mirror scattering. The scattering mechanism is very complex and difficult to model and estimate. Therefore, it is important to study the scattering mechanism in this area.

The large-diameter concave structure at the nose cone is the most important scattering mechanism. The engine air intake is a typical concave-cavity structure. Since scattering comes from multiple interaction between the wall, flow deflector and compressor blade, it is very difficult to simulate using conventional methods.[4] In addition, if the target has an automatic-homing nose cone, its final guidance antenna and radar compartment also form a complex concave structure. The scattering mechanism of an antenna is even more complicated than that of an ordinary object. Because an antenna is a

loaded scattering object, in addition to the structure-scattering term σ_s, there is a mode-scattering term σ_a due to load mismatch. Therefore, the total RCS of an antenna is:[3]

$$\sigma = \left| \sqrt{\sigma_s} + \sqrt{\sigma_a} \exp(j\psi) \right|^2 \qquad (2)$$

where ψ is the relative phase difference between the two scattering terms. Based on antenna theory, it is possible to derive an approximate formula to estimate the maximum RCS of an antenna[5] as follows:

$$\sigma_{max} = (1/\pi)\, G^2\lambda^2 \qquad (3)$$

where G is the gain of the antenna and λ is the operating wavelength.

If the flying object has no nose cone and air intake, then various discontinuities at the leading and trailing edges of the wings and the tail become the major scattering mechanism. They can be treated by geometric diffraction theory. The mirror reflection from the nose of the flying object is also a conic sector scattering mechanism and can be estimated by geometric optics.

Another important scattering mechanism from the conical sector is the scattering of surface traveling waves. When an incident radar wave excites a slender object, if there is an incident electric field component along the direction of propagation on the surface, there is a surface current traveling wave. When the forward traveling wave meets a discontinuous structure (e.g., tail end, wing tip), the reflected traveling wave will produce an effective scattering echo in the nose-cone sector. It may be three orders of magnitude larger than that of the mirror echo from geometric optics.[6] Unfortunately, the research on this scattering mechanism is not sufficient; it is not possible to use a simple formula to quantitatively determine the scattering intensity.

III. Theoretical Analysis of RCS

The RCS of a target is a complex physical quantity. It is dependent upon geometric and material characteristics of the target such as shape, dimensions and structure, as well as its electrical parameters. It is also related to the direction, wavelength and polarization of the incident wave. Using electromagnetic scattering theory and modern computer technology to estimate target RCS is an effective means in the study of target characteristics and stealth technology.

In principle, all electromagnetic scattering methods are applicable to RCS calculation. However, in practice the classical boundary-value method and integration-equation-moment method are useless for large targets. Only various high-frequency approximation methods are effective.[2,4] The geometric optics method and geometric diffraction method can provide satisfactory estimates for curved mirror reflection and straight and curved-edge diffraction. Their inadequacy in transition and caustic zones can be corrected by a consistent diffraction method and effective electromagnetic current method, respectively. The physical optics method integrates the scattering field of surface-induced current and simplifies the process by using the standing phase principle. Satisfactory results can be obtained in the mirror direction. It may be expanded to any direction by using diffraction theory and the incremental-length diffraction coefficient. The plane-wave spectrum method employs Fourier transforms to convert the aperture field integral to a spectrum integral and uses the saddle-point method to compute the integral in approximation. The microwave network method is based on transmission-line theory or waveguide theory and may be used to analyze the scattering characteristics of certain structures.

Numerous studies have been conducted throughout the world. Satisfactory results have been obtained in estimating the scattering characteristics and RCS of most metallic targets. Nevertheless, there are still many challenging problems remaining involving a number of actual structures, such as dielectric antenna housings, wave-absorbing coatings and composite-material structures, antennas (re energy absorption and scattering), and concave structures such as air intakes and exhaust; there is also the problem of surface-traveling-wave scattering. They are either hard to model theoretically or difficult to compute numerically; some new methods therefore need to be developed.

The complex ray theory developed in recent years[7,8] can simplify the calculation of certain targets. For instance, the complex-ray near-axis approximation method and collective-ray method can simplify the RCS calculation of layered dielectric targets (such as radomes, wave-absorbing coatings and composite wings).[9,10] As for large-diameter concave structures such as air intakes, tail exhausts, bifacial wing angles, cockpits and antenna and radar housings, a complex-ray expansion method may be used[11,12] to simplify complex-ray tracking and field-strength calculation. More accurate RCS results have been obtained. Figure 2 shows the modeling and experimental results of an 84 x 110 mm^2 curved air inlet.[13,14] The dotted curve is the calculated result, which is in good agreement with the solid-line experimental data. The line-dot curve is the result from a waveguide model. Obviously, its accuracy is poor.

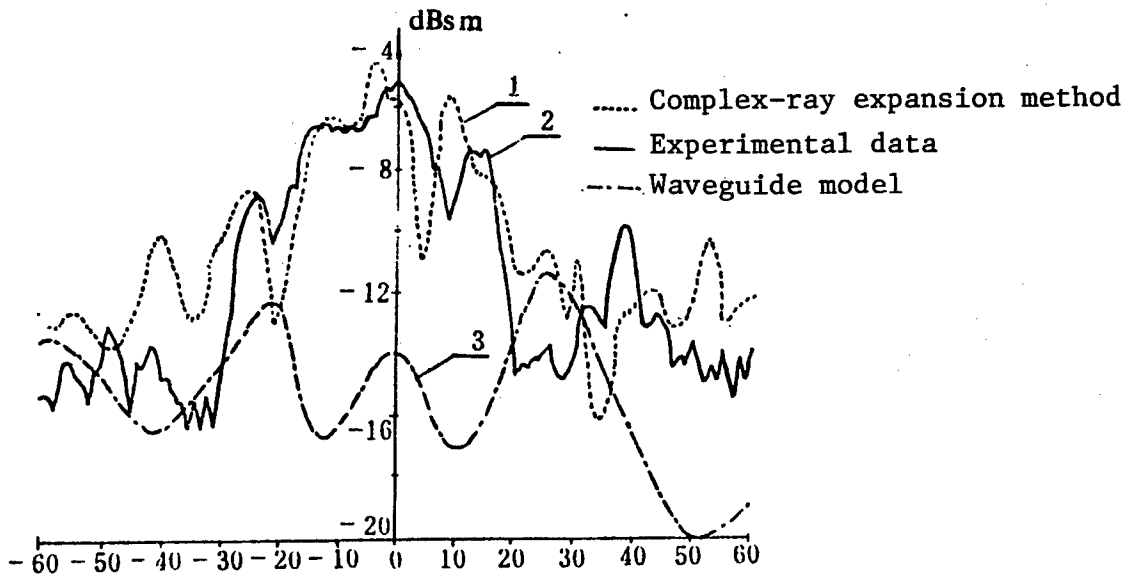

Figure 2. RCS of S Tube With Rectangular Cross Section (λ = 3.2 cm, horizontally polarized)

IV. RCS Reduction and Stealth Technology

The purpose of RCS research is to control target scattering in order to reduce RCS in the direction of hostile radar. With regard to high-frequency scattering from a complex target, the first problem is to identify flickering points that generate intense scattering so that effective measures can be taken to suppress scattering. After strong scattering points are eliminated, some secondary or weak scattering mechanisms will become predominant factors. Hence, there is an increasingly costly price to pay in RCS reduction technology which involves constraints in manpower, financial resources, dimensions, weight and structure. Furthermore, its optimization involves a compromise of a number of factors including stealth, aerodynamics, control and guidance, and cost.

It is generally believed that radar wave-absorbing materials, external profiling and loading cancellation are three viable ways to reduce RCS. Nevertheless, these basic RCS reduction techniques will develop into different forms depending upon the target, scattering mechanism, and direction, frequency and polarization of the incoming wave.

On the side, wave-absorbing materials are the most effective way to suppress mirror reflection. A magnetic wave-absorbing material made of ferrite iron carbonyl powder has been widely coated on the surface of airplanes. Upon normal incidence onto a planar structure at the central frequency, this material can reduce reflectance by 20-30 dB. However, away from the central frequency, or coming at an angle, or onto a curved surface, the wave-absorbing effect falls off very rapidly. This is an urgent issue in the study of wave-absorbing materials. Although the frequency bandwidth can be expanded by using a structure with multiple layers which resonate at different frequencies, its use is limited by weight and thickness. Another direction in wave-absorbing materials is to develop novel composite materials to replace metallic components. It is estimated that more than one-half of structural materials used on military aircraft will be made of new wave-absorbing composite materials by the end of this century.

External profiling is another effective means to suppress scattering. This stealth mechanism is not based on energy absorption. Instead, energy is scattered outside the coverage area of the hostile radar by the external profile design. The use of wing-fuselage merging techniques, buried cockpits, V-shaped oblique tails, and elimination of tail and rudder are effective techniques to suppress strong bifacial-angle scattering. Delta wings, variable sweptforward or sweptback wings, and use of absorbent materials at the edges can significantly reduce the diffractive contribution of wing edges. Using internal weapon hangers and eliminating pods and protruding edges can further reduce target scattering at the nose cone. These techniques have been successfully used in the design of U.S. military aircraft. Stealth profiling technology is closely related to aircraft system design and some compromises are required.

In order to reduce the RCS of the nose cone, measures are first taken to improve key scattering sources such as the inlet and antenna. Changing the conventional straight air intake to a curved or variable cross-section inlet is an effective stealth method. As shown in Figure 2, the RCS of the S-shaped inlet is approximately 5 dB lower compared to that of a straight tube. Installing reflective screens on the radial surface of the inlet, adding an electromagnetic wave-interference device in the tube, inserting dielectric grids or applying absorbent

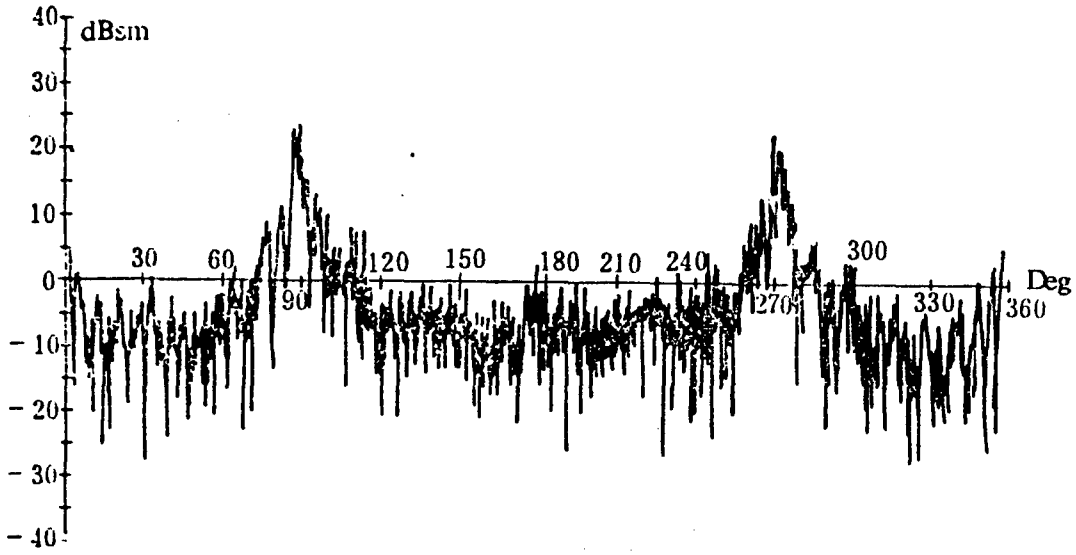

Figure 3. Measured RCS Directional Pattern of a Typical Target With Antenna Disguise Cover

coatings on the inner wall, and using piggyback or slotted air intakes can also reduce backscattering of the nose cone. However, all these measures must not disturb the flow field distribution of the inlet and thrust performance of the aircraft.

In order to suppress antenna scattering in the nose-cone direction, the simplest and most effective method is to use an antenna disguise technique. When it is not operating, the antenna is pointing away from the nose cone. Or, a low-RCS cover is used. The disguise cover may be metallic or have a frequency-selective surface or a polarization-selected structure. Figure 3 shows a RCS directional pattern of a missile model with a disguise cover. The echo from the nose cone is significantly reduced and the peak RCS is lowered by approximately 10 dB. Frequency-selection and polarization-filtering techniques can also be used in the design of antenna reflective surfaces. Precision matching techniques can be used in the design of antenna feed sources. These methods can further reduce antenna scattering.

Compared to a reflective surface antenna, an array antenna system has a lower RCS. Using high-gain low-RCS emitting elements, changing a flat array into a curved array or conformal array, using digital phase-shifting devices and computers to realize phase-controlled scanning and adaptive beam-forming can also lower the contribution to the RCS of the antenna. However, these measures will increase complexity and cost.

There was a great deal of interest in loading cancellation technology in the 1960's. Scattered echo from passive loads can cancel the scattering from other parts. For instance, slots may be opened on conductive surfaces such as the wing. The amplitude and phase of this artificial scattering can be adjusted by connecting to cavities to reach a certain total impedance. An admittance adjustment plate may be added to the antenna waveguide to have its mode term and structure term cancel each other. Adjusting the size and position of the secondary reflective surface can make the main and secondary reflective surface cancel each other. Adjusting the depth of the main reflective surface may cause mirror reflection and edge diffraction to cancel each other.[15] However, all passive cancellation techniques are limited by frequency band, polarization and incident direction. To obtain cancellation effects of practical value, it is necessary to use an adaptive active loading technique. Based on the intensity, waveform, frequency, polarization and incident direction of the hostile radar detected, the reflection characteristics of the target are quickly calculated. Then, the waveform, amplitude and phase of the artificially added pulse are immediately adjusted to obtain the optimal RCS reduction. Due to the complexity of technology and equipment involved, this technique has not been used in any weapons system.

Anti-radar stealth technology often employs a number of techniques mentioned above. It was estimated that an optimal profile design could have a 5-8 dB effect. Wave-absorbing materials could reduce RCS by 7-10 dB. Special measures such as air intakes, antennas and passive loading could lower it by 4-6 dB each. Through a combination of various techniques, modern military aircraft has achieved a stealth effect of over 20 dB. The B-2 bomber is a milestone in the modernization of the U.S. Air Force. Figure 4 shows its external appearance. The aircraft is 21 m long and 5.2 m high. Its wingspan is 52 m. It has delta wings but no tail. It has a sawtooth-shaped trailing edge. The leading edge uses a honeycomb structure made of an absorbing material. Its surface is

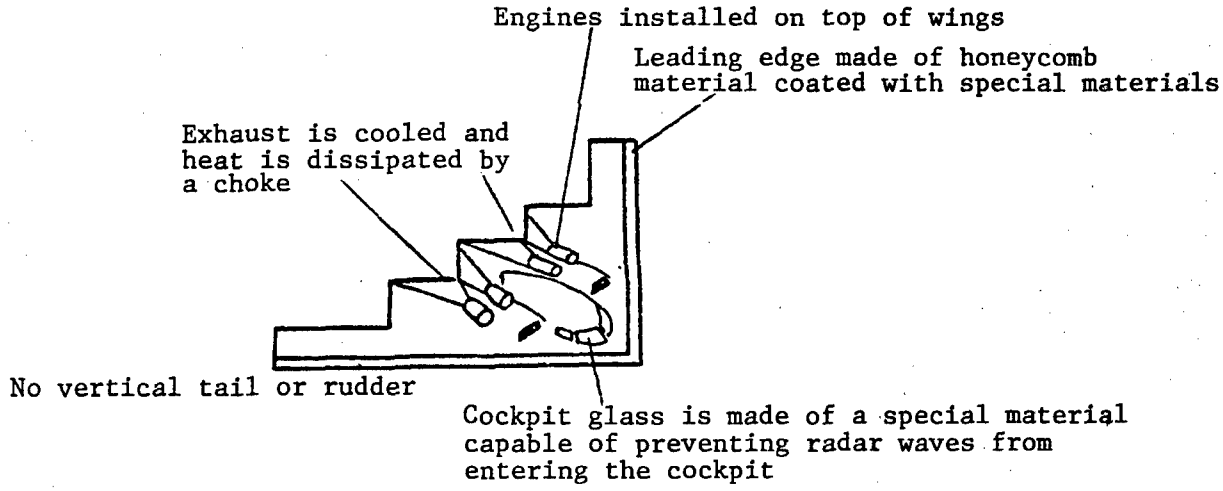

Figure 4. External Profile of the B-2 Bomber

coated with a wave-absorbing film. Composite fiber-reinforced carbon and epoxy materials are used internally. Four engines are mounted on top of the wings. The canopy is made of a transparent glass capable of reflecting microwaves. There is no vertical tail or rudder. After taking these measures, it was reported that its RCS is only 0.3-0.5 m^2. Compared to B-52, it has achieved a 23-25 dB stealth effect.

V. Counter-Stealth Detection Technology

In order to deal with developing stealth technology, counter-stealth theory and technique are also being investigated. However, they are far from being as mature as stealth technology. Currently, counter-stealth technology is primarily focused on problems associated with stealth technology. New radar systems or electromagnetic scattering theories are used to detect low-RCS targets.

An effective counter-stealth method is to build an air-defense radar network over a very wide frequency range. Since the present stealth measures (especially wave-absorbing materials) are primarily for centimeter-wave radar, the RCS reduction effect falls off rapidly with increasing and decreasing frequency. Therefore, developing millimeter-wave and sub-millimeter-wave radar at the high-frequency end and meter-wave and centimeter-wave radar or short-wave over-the-horizon radar at the low-frequency end can lower the effectiveness of the stealth effect. In addition, it is very hard to jam a wide-band air-defense radar network. This is what we need to counter aircraft with both stealth and radar-jamming capability.

Further improvement of existing radar systems can also suppress stealth effects to some extent. Increasing transmission power is undesirable because it increases the probability of exposure. More advanced signal-processing techniques should be used to improve the detection capability. An adaptive detection scheme for the polarization characteristics of scattered waves from the target should be used. Based on the phase-coherence behavior of a multiple-scattering center, a multi-channel receiver system is used to adaptively adjust amplitude and phase in order to superimpose the same phase. Synthetic aperture and inverse synthetic aperture theories are used to raise the cumulative number of pulses of similar parameters. Pulse compression techniques can be used to raise the mean transmission power while ensuring the range resolution. These measures can improve the detection capability of existing radar systems of low-RCS targets.

Since most stealth measures are taken specifically against a single radar station below, it is not difficult to detect existing stealth airplanes by constructing a dual or multiple radar station system or developing airborne early-warning platforms with downward-looking capability.

Developing passive electronic transducers such as passive radar and infrared sensor technology are also effective ways to counter low-RCS targets. A highly sophisticated system can receive sufficient information from the electromagnetic radiation and thermal radiation from a stealth aircraft to complete a number of passive measurements such as location and speed. Passive systems are receiving more attention than active radar systems.

New theories in electromagnetic scattering and backscattering can be used to develop some novel target detection and identification techniques. For example, a radar without a carrier frequency can be developed based on the impact effect of the target in response to a very narrow single-cycle wave. The pole and natural resonant frequency of the target can be extracted by an oblique-rise response method or singularity-expansion method. In addition, the scattering characteristics of the target are

used to analyze the scattering field and to process backscattering in order to achieve target detection and identification. These new theories and techniques are still in an exploratory stage and are some distance away from being used in the field.

VI. Conclusions

Stealth technology, developed based on target scattering characteristics and RCS studies, and high-energy laser weapons and cruise missiles are the three major technical innovations in military science in the 1980's. They will bring new dimensions to weapons development in the 1990's and in future wars. In addition, they will promote new developments in a series of technical fields such as aeronautics, astronautics, mechanical engineering, electronics, computer science, chemical engineering and materials science. There are still a large number of challenging theoretical topics and key technical issues to be resolved in stealth and counter-stealth technology. Various nations are conducting additional studies on these subjects.

The author wishes to thank Professors Lin Weigan [2651 3634 1626] and Xie Chufang [6200 5710 2455] for their concern and guidance.

References

1. Ruan Yingzheng and Lin Weigan, DIANZI KEXUE JISHU [ELECTRONIC SCIENCE AND TECHNOLOGY], Vol 18, No 11, pp 2-4, 1988 [see JPRS-CST-89-007, 17 Mar 89, pp 72-78].

2. E. F. Knott, et al., "Radar Scattering Cross Section" (Ruan Yingzheng, et al., editors), Electronics Industry Publishing House, Beijing, 1988.

3. G. T. Ruck ed., "Radar Cross Section Handbook," Vol 2, Plenum Press, New York, pp 530-670, 1970.

4. E. F. Knott, PROC. IEEE, Vol 73, No 2, pp 252-264, 1985.

5. Ruan Yingzheng, "Scattering Mechanism and RCS Reduction of Antennas," YUHANG XUEBAO [JOURNAL OF CHINESE SOCIETY OF ASTRONAUTICS], Vol 11, No 4, Oct 90, pp 94-100 [see full-text translation above].

6. J. W. Crispin, Jr., and A. L. Maffett, PROC. IEEE, Vol 53, No 8, pp 833-848, 1965.

7. Ruan Yingzheng, TONGXIN XUEBAO [JOURNAL OF CHINA INSTITUTE OF COMMUNICATIONS], Vol 8, No 4, pp 51-59, 1987.

8. Ruan Yingzheng, "Fundamental Electromagnetic Radiation Theory," Chengdu Institute of Telecommunications Engineering Press, 1989, Chapter 5.

9. Ruan Yingzheng and L. B. Phearson, YINGYONG KEXUE XUEBAO [JOURNAL OF APPLIED SCIENCE], Vol 7, No 2, pp 174-178, 1989.

10. Ruan Yingzheng, DIANZI XUEBAO [ACTA ELECTRONICA SINICA], Vol 17, No 3, pp 89-94, 1989.

11. Ruan Yingzheng, CHENGDU DIANXUN GONGCHENG XUEYUAN XUEBAO [JOURNAL OF CHENGDU INSTITUTE OF TELECOMMUNICATIONS ENGINEERING], Vol 16, No 1, pp 28-33, 1987.

12. Ruan Yingzheng, GUANGXUE XUEBAO [ACTA OPTICA SINICA], Vol 8, No 1, pp 83-88, 1988.

13. Feng Wenlan [7458 2429 3482] and Ruan Yingzheng, "RCS Analysis of Coiled Air Intake," YUHANG XUEBAO [JOURNAL OF CHINESE SOCIETY OF ASTRONAUTICS], Vol 11, No 6, pp 276-280, 1990.

14. Ruan Yingzheng, YINSHEN JISHU [STEALTH TECHNOLOGY], Vol 3, No 1, pp 18-27, 1989.

15. P. S. S. Kao, AD770012, 1973.

Analysis of Electromagnetic Characteristics of 3-D Dielectric Radome by Complex Astigmatic Wave Theory

91FE0306A Beijing DIANZI KEXUE XUEKAN [JOURNAL OF ELECTRONICS] in Chinese Vol 12 No 6, Nov 90 pp 561-568 [MS received 20 Nov 89, revised 7 Apr 90]

[Article by Wang Yueqing [3769 2588 3237] of the Naval Institute of Electronic Engineering, Nanjing: "Analysis of Electromagnetic Characteristics of 3-D Dielectric Radome by Complex Astigmatic Wave Theory"]

[Excerpts] **Abstract**

Complex astigmatic wave theory is an effective method for analyzing the electromagnetic characteristics of 3-D radomes. In this work, numerical results of an ellipsoidal radome are expressed in terms of stereoscopic graphs. Compared with experimental results, this method can effectively simplify the analysis, calculation and design optimization of dielectric radomes.

I. Introduction

Developments in modern aeronautic and astronautic technology have imposed very demanding requirements for radomes. In addition to meeting aerodynamic and mechanical properties, electrical properties must also be satisfied.[1] However, due to the presence of the dielectric interface of the radome, the directivity diagram of the antenna must be distorted and the inherent characteristics of the radar are affected. Therefore, methods for designing satisfactory radome from theoretical analysis and optimization calculation has attracted a great deal of interest. The study of the electromagnetic properties of radomes involves transmission and scattering of high-frequency electromagnetic waves in dielectric layers. Conventional methods such as the geometric optics method, physical optics method, plane-wave-spectrum surface integration method and microwave network

method are often used.[2] However, difficulties are encountered in numerical analysis and integration involving 3-D radomes with arbitrary curvature and structure. In this paper, spatial geometry and complex astigmatic wave theory are used to study the electromagnetic characteristics of an arbitrary 3-D radome in order to avoid complicated field integration. Furthermore, theoretical analysis and numerical results of an ellipsoidal sandwich radome are shown as an example and compared with experimental data. It was found that complex astigmatic wave theory is an effective way to analyze the 3-D propagation and scattering of focused beams. [passage omitted]

IV. Numerical Analysis

Based on the complex astigmatic wave theory described above, computer modeling for the ellipsoidal radome shown below in Figure 2 is performed. Its medium interface equation is:

$$r_i = (x, y, c_i \sqrt{1 - x^2/a_i^2 - y^2/b_i^2} - 500) \quad (21)$$

where i = 1, 2, 3, 4, represents the interface layer number; $a_1 = b_1 = 265$ mm, $c_1 = 1{,}295$ mm; $a_2 = b_2 = 265.5$ mm, $c_2 = 1{,}295.5$ mm; $a_3 = b_3 = 269.5$ mm, $c_3 = 1{,}299.5$ mm; $a_4 = b_4 = 270$ mm, $c_4 = 1{,}300$ mm; dielectric constant of the medium $\varepsilon_1 = \varepsilon_3 = 3.2$, $\tan \delta_1 = \tan \delta_3 = 1.4 \times 10^{-3}$; $\varepsilon_2 = 1.08$, $\tan \delta_2 = 2.4 \times 10^{-3}$; operating wavelength $\lambda = 31.689$ mm; complex astigmatic wave width parameter $b_H = 333.28$ mm, $b_E = 1{,}327.5$ mm, phase center position $\Delta_H = 4.6\lambda$ and $\Delta_E = 1.4\lambda$.

Under the above experimental conditions, sum-and-difference wave-penetration directivity diagrams of the radome were calculated and measured. Figure 3(a) shows the measured and calculated directivity diagrams on the H-plane when the sum wave penetrates the ellipsoidal radome and in the absence of the radome when $\zeta_s = 0°$. The figure shows that the theoretical and experimental results are in good agreement for the main lobe. Its accuracy coincides with the error analysis. However, there is some error on the side lobe. Nevertheless, this error is acceptable for engineering applications when applying this theory to the study of scattering and propagation properties in three dimension.

Figure 3(b) and (c) represent theoretical values of 3-D stereoscopic graphs of the sum wave without and with

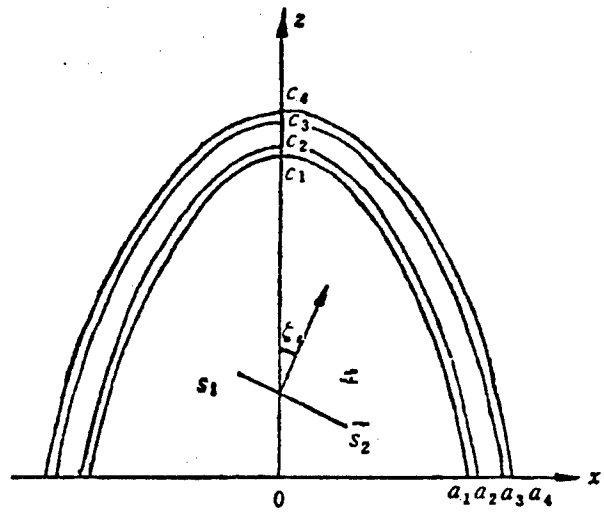

Figure 2. Ellipsoidal Sandwich Radome Structure

the radome, respectively. In these figures, x and y are the rectangular coordinates of the observation point P (x, y, z). Further, $x^2 + y^2 + z^2 = R^2$, where R is the spherical radius of the observation region. Its transmission coefficient is K = 97.21 percent. This shows that this ellipsoidal sandwich radome has a considerably high transmittance in the nose-cone direction.

Figure 4(a) shows directivity diagrams of the difference-wave radiation field and penetration field through the radome on the H plane with $\zeta_s = 0°$. Because $\zeta_s = 0°$, the penetration field does not produce any angular deflection due to system symmetry.

Figure 4(b) and (c) show the theoretical results of the difference-wave scattering field and penetration field across the radome. Thus, the 3-D directivity diagram of the difference wave can be visualized.

Figures 5 and 6 show the theoretical and experimental results of the scattering field and penetration field on the H plane for the sum-and-difference wave and its theoretical stereoscopic graph at $\zeta_s = 15°$. Since the transmitting antenna is not symmetric with respect to the radome at this emission angle, an angular deflection is resulted. The zero depth rises and difference slope declines. Consequently, radar performance deteriorates.

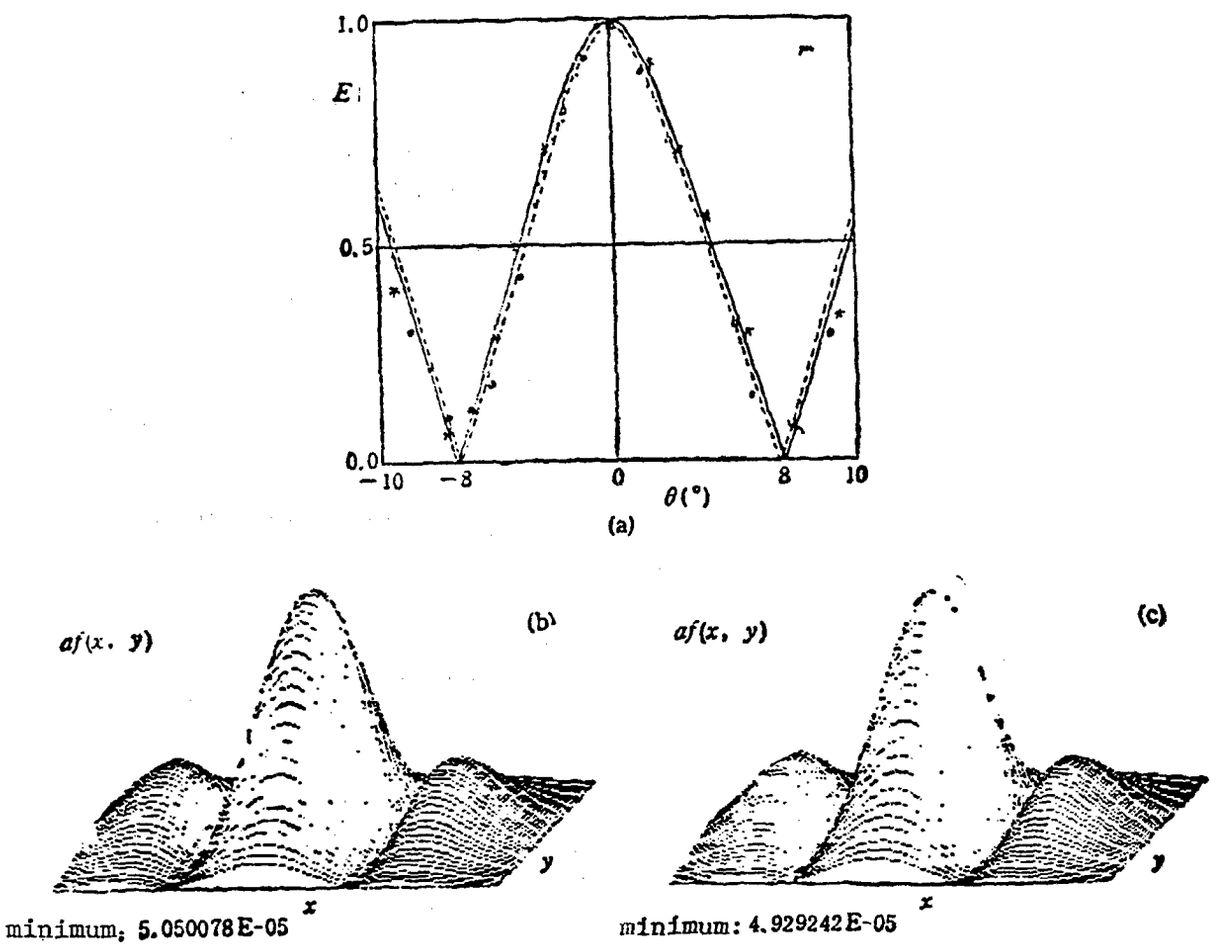

Figure 3. Calculated and Measured Directivity Diagrams for an Ellipsoidal Radome at $\zeta_s = 0°$

(a) Comparison of theoretical and experimental sum-wave-penetration field values on the H plane. Solid line—theoretical sum-wave value without radome, broken line—theoretical sum-wave field after penetrating the radome; xxx—experimental sum-wave value without radome, ooo—experimental sum-wave-penetration field. (b) 3-D sum-wave stereoscopic graph without radome (theoretical). (c) 3-D sum-wave stereoscopic graph with radome (theoretical).

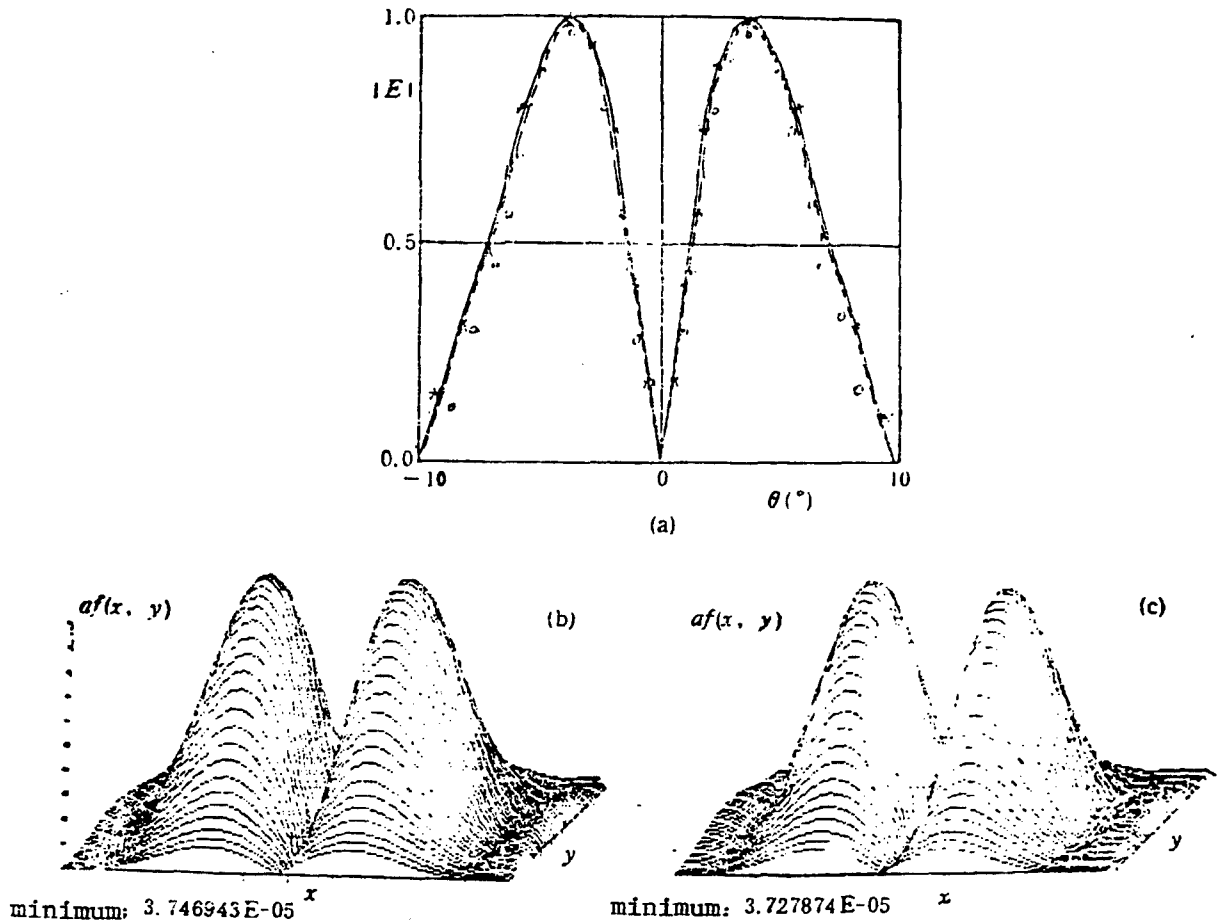

Figure 4. Calculated and Measured Directivity Diagrams for an Ellipsoidal Radome at $\zeta_s = 0°$

(a) Comparison of theoretical and experimental difference-wave penetration field values on the H plane. Solid line—theoretical difference-wave value without radome, broken line—theoretical difference-wave field after penetrating the radome; xxx—experimental difference-wave value without radome, ooo—experimental difference-wave penetration field. (b) 3-D difference-wave stereoscopic graph without radome (theoretical). (c) 3-D difference-wave stereoscopic graph with radome (theoretical).

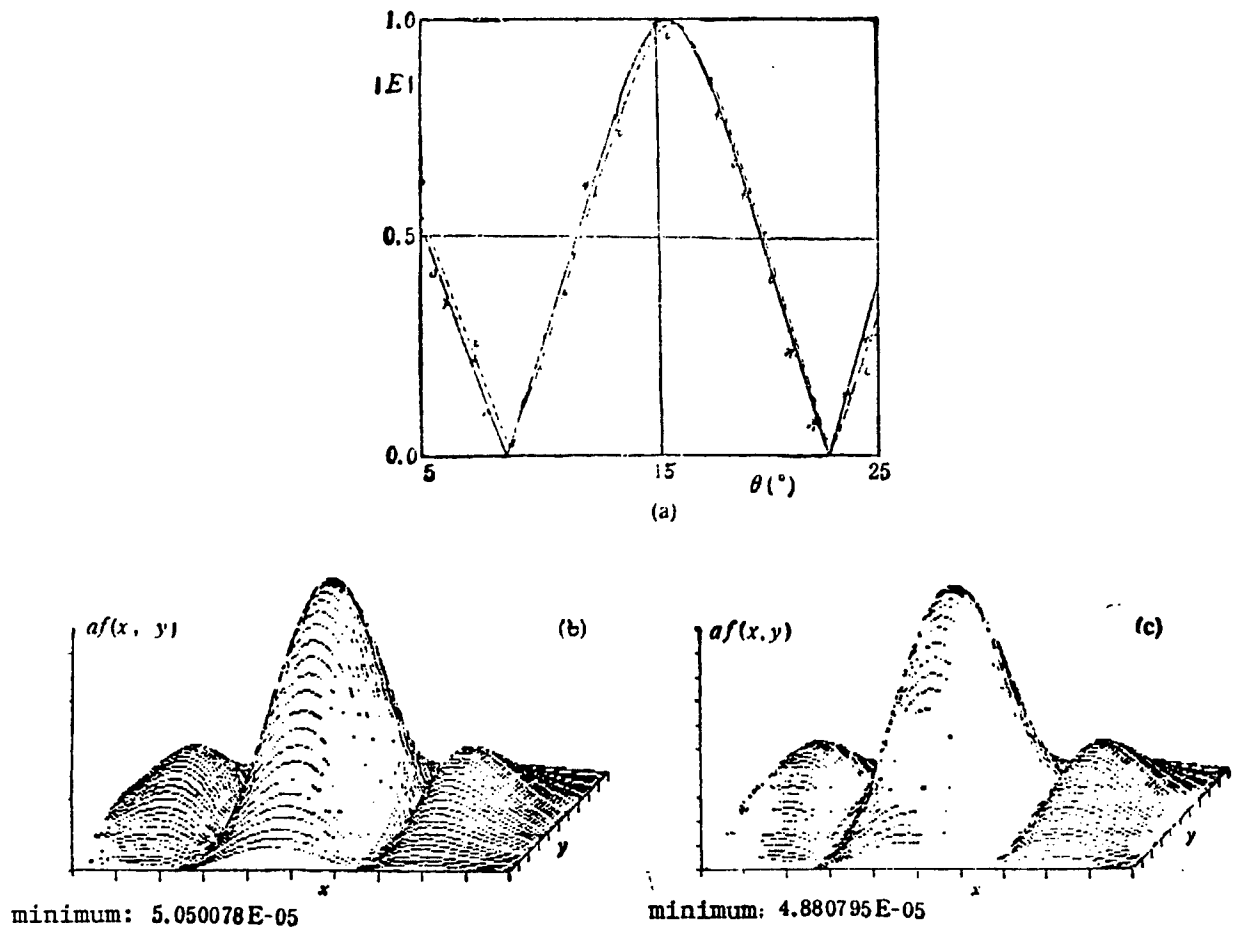

Figure 5. Calculated and Measured Directivity Diagrams for an Ellipsoidal Radome at $\zeta_s = 15°$

(a) Comparison of theoretical and experimental sum-wave penetration field values on the H plane. Solid line—theoretical sum-wave value without radome, broken line—theoretical sum-wave field after penetrating the radome; xxx—experimental sum-wave value without radome, ooo—experimental sum-wave penetration field. (b) 3-D sum-wave stereoscopic graph without radome (theoretical). (c) 3-D sum-wave stereoscopic graph with radome (theoretical).

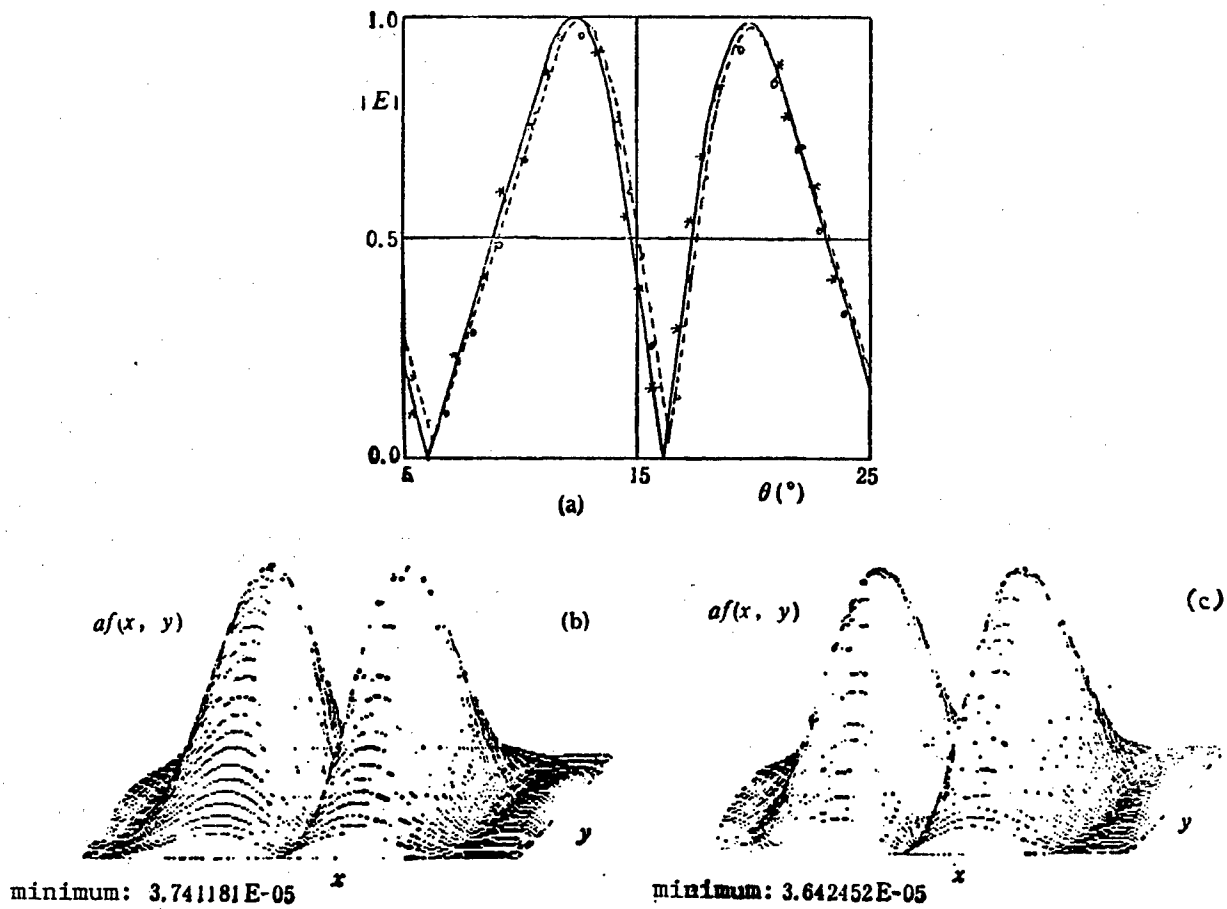

Figure 6. Calculated and Measured Directivity Diagrams for an Ellipsoidal Radome at $\zeta_s = 15°$

(a) Comparison of theoretical and experimental difference-wave penetration field values on the H plane. Solid line—theoretical difference-wave value without radome, broken line—theoretical difference-wave field after penetrating the radome; xxx—experimental difference-wave value without radome, ooo—experimental difference-wave penetration field. (b) 3-D difference-wave stereoscopic graph without radome (theoretical). (c) 3-D difference-wave stereoscopic graph with radome (theoretical).

V. Conclusions

The complex astigmatic wave theory used in this work expands the use of such a technique from 2-D or main plane problems to 3-D, providing some theoretical basis for realistic modeling of focused beams. It makes the study of propagation and scattering of focused beams in a complicated environment possible. However, because this complex astigmatic wave theory is based on geometric optics, it is only applicable to high-frequency electromagnetic wave fields. In addition, this focused-beam model is only used to simulate the scattering and transmission on the main lobe, which also limits the range of applications of this theory.

As a developing theory, there are still many problems to be resolved. For instance, the analysis of electromagnetic astigmatism of a dielectric medium and the transmission mechanism of complex astigmatic waves in medium with loss, dispersive medium, and anisotropic medium need to be investigated.

The author wishes to thank Professors Xie Chufang [6200 5710 2455] and Ruan Yingzheng [7086 4481 6927] of the University of Electronic Science and Technology of China for their guidance and support.

References

1. G. A. E. Crone, A. W. Rudge, and T. N. Taylor, IEE PROC., Part F, 128 (1981), 7, 451-464.

2. P. C. Wilcockson, "Radome Design and Their Properties: A Review," IEE CONF. PUBL. 77 (1971), pp 212-218.

3. Erwin Kreyszing, "Differential Geometry," Toronto University of Toronto Press, London, Oxford University Press, 1959, 72-174.

4. Y. Z. Ruan and L. B. Felsen, J. OPT. SOC. AM. A., 3 (1986) 4, 566-579.

Analysis of Target RCS by Complex Ray Expansion

91FE0306B Beijing DIANZI KEXUE XUEKAN [JOURNAL OF ELECTRONICS] in Chinese Vol 12 No 6, Nov 90 pp 646-649 [MS received 12 Feb 89, revised 27 Oct 89]

[Article by Feng Wenlan [7458 2429 3482] and Ruan Yingzheng [7086 4481 6927] of the University of Electronic Science and Technology of China, Chengdu, project funded by the Doctoral Foundation of the State Education Commission and Institute of Electronics of MMEI: "Analysis of Target RCS by Complex Ray Expansion"]

[Excerpts] **Abstract**

This paper presents a simple method for calculating the scattering characteristics of a complex target based on complex-ray analysis and Gaussian-beam expansion of the field. Because the complex-ray method is not limited by target shape, this method may be used with any target. In this paper, a rectangular air intake is used as an example to calculate its radar cross section (RCS). Comparison of the calculated values with the measured results indicates that this method is feasible.

1. Introduction

With the advancement of stealth technology, in order to study the electromagnetic scattering characteristics of military targets, computation of RCS has received a great deal of attention. The methods used include the geometric optics method, physical optics method, geometric diffraction method, planar-wave spectroscopy method and microwave network method. These methods are effective in dealing with simple targets and small-scale models. However, complicated boundary conditions and realistic-size targets will be limited by computer memory, computation time and complexity of equations. [passage omitted] The purpose of this study is to explore the feasibility of using Gaussian-beam expansion and complex-ray analysis[1-3] to calculate the RCS of a complex target.

2. Gaussian-Beam Expansion and Complex-Ray Method

From complex-ray analysis,[3] a complex point-source field is a focused beam toward a fixed direction in real space. It falls off rapidly on both sides of the axis like a Gaussian function. Therefore, when the incident field is the scattering field of a needle-shaped beam (e.g., radar beam), a Gaussian beam is a very good approximation. Hence, the electromagnetic scattering characteristics of the target can be calculated by complex-ray theory. However, when the target is far away from the transmitting radar, the target receives a near-planar-wave field. In this case, it is not possible to use a Gaussian beam to approximate a plane-wave field. It is necessary to expand the plane wave into a Gaussian function to use complex-ray theory for analysis.

As for Gaussian expansion, there is not yet a precise way to solve this problem.[1-4] Function expansion is a pure mathematical problem. To expand a function into a linear combination of another series of functions, the key is to solve the expansion coefficients.

A basic Gaussian function can be expressed as

$$G(x) = (\sqrt{2}/T)^{1/2}\exp[-\pi(x/T)^2] \qquad (1)$$

Because a Gaussian function is not orthogonal,[5] in order to expand a function into the sum of a series of Gaussian functions, the expansion coefficients cannot be determined one by one. It is not possible to express it by an analytical equation. Since the 1980's, some researchers have been using biorthogonal functions to investigate the expansion of a Gaussian beam, such as Hermite-Gauss expansion and Laguerre-Gauss expansion.[4] These

biorthogonal-function expansions are Gaussian-modulated orthogonal expansions. Nevertheless, the pure-Gaussian-expansion problem has not been solved.

This work uses a fitting method to expand a plane wave into a Gaussian wave (complex-point-source field). Because the signal received by a target from a distant radar is a uniform plane wave, it may be expressed by a series of uniform complex point sources of equal amplitude and phase. As shown in Figure 1, let us assume that E_i is the uniform plane wave received by the target, s_0, s_1, s_2.... are a series of point sources with beam vector b and spacing Δy^2. By properly selecting b and Δy, it is possible to make the summation equation have a sufficient fitting accuracy.

$$E_i \approx \sum_l \frac{C}{\sqrt{kR}} \exp(kb) \exp\left[\frac{k(y - l\Delta y)^2}{2b}\right], \quad (l \text{ is an integer}) \quad (2)$$

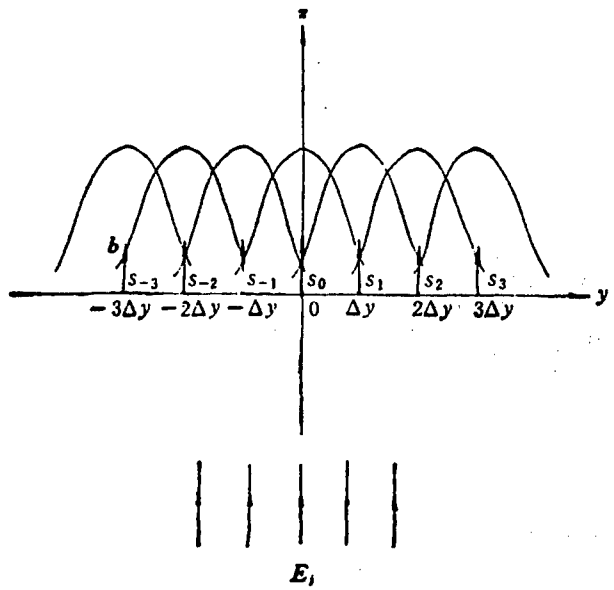

Figure 1. Gaussian Beam Fitting of a Uniform Plane Wave

With these equivalent complex-point sources, complex-ray theory can be used to analyze the electromagnetic scattering of the target. In near-axis complex-ray approximation,[2] based on the attribute of the real part of the center complex ray, the tedious searching process can be avoided. The axial field can be determined simply by using the real ray trajectory:[6]

$$E_{P_0} = -\frac{\omega\mu_0}{\sqrt{8\pi j\tilde{k}_0\tilde{L}_1}} \tilde{T}_M \tilde{D}_M e^{j\tilde{k}_0\tilde{\varphi}_M} \quad (3)$$

where [tilde]L_1 is the optical path traveled by the center complex ray before scattering upon meeting any obstacle or medium interface, [tilde]T_M is the overall complex transmission coefficient, [tilde]D_M is the overall complex diffusion factor, and [tilde]φ_M is the total optical path along complex-ray scattering. After the axial field is found, then complex-phase and complex-amplitude correction are made for the beam axial field based on the perturbation principle.[6] The approximate field at any observation point away from the main axis can be determined. As shown in Figure 2, the field at point P_0 on the main axis is known. Then, the field at point P off the center axis is:

$$E_P \approx E_{P_0} \exp(j\tilde{k}_0 \Delta\tilde{L}) \quad (4)$$

where Δ[tilde]$L = d^2/(2[\text{tilde}]D_{ro}) = d^2/[2([\text{tilde}]f_0 + L_{ro})]$; $d = \overline{PP_0}$ is the perturbation distance; [tilde]f_0 is the complex distance between the imaginary image point [tilde]F_0 to the point of reflection [tilde]A; L_{ro} is the distance between the point of reflection to point P_0 on the axis.

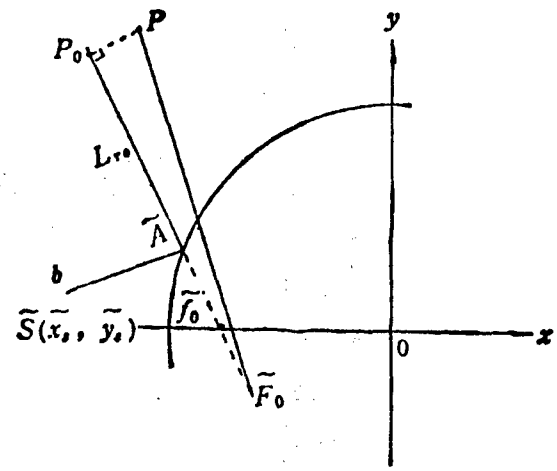

Figure 2. Perturbation Principle of Complex Ray

It needs to be pointed out that in complex-ray expansion it is necessary to track and calculate every complex point source and the fields must be summed up to determine the total field at the observation point. However, because of the fast drop-off of the point source field, not all points are contributing to the field at a specific observation point. Therefore, integration or summation is carried out within a finite range. Thus, computation can be simplified to raise the speed.

3. Numerical Results

Figure 3 shows a 255-mm-long metal air intake with a 57 mm x 57 mm rectangular cross section. The figure also shows the track of a ray. A 1,500-line program in C language on an IBM PC/XT was written for ray-tracking and field-summation. Figure 4 shows the calculated results for the model shown in Figure 3; it is compared to the experimental and calculated results reported in references 7 and 8. From

the figure, the results calculated in this work coincide better with the experimental data. Figures 5 and 6 are the 241 RCS values calculated between -60° and +60° at 0.5° apart under vertical and horizontal polarization, respectively. From the figure, the overall RCS varying tendency agrees with measured results. Because the ray reflects many times in the air intake, when the angle varies slightly, RCS fluctuates quite a bit. In addition, the advantage of the method is its fast speed. Total computation of RCS over the range from -60° to +60° with 2° increments (results shown in Figure 4 are 2° apart) only takes 124 s of CPU time. On the average, it takes approximately 2 s to track and sum each point. This is very important for treating more complicated targets.

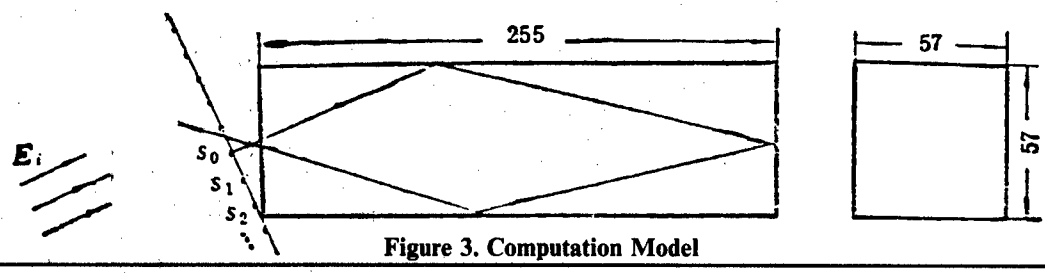

Figure 3. Computation Model

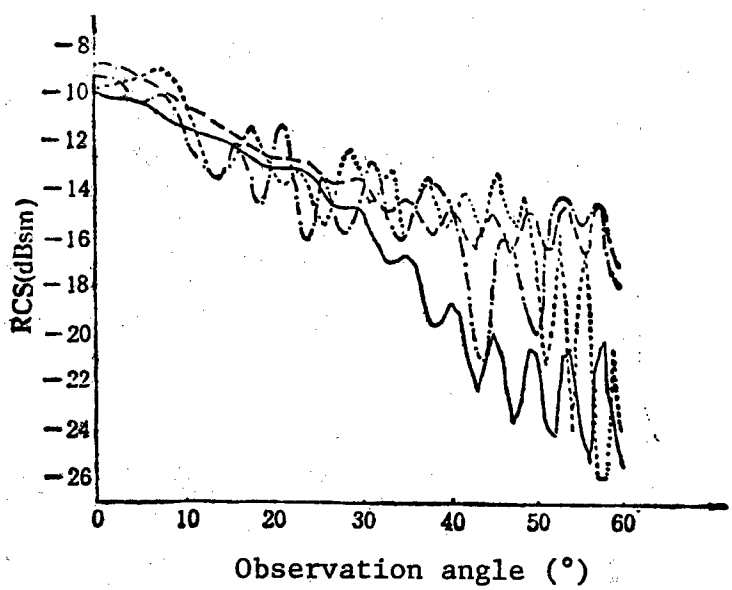

Figure 4. Calculated Results of Model Shown in Figure 3 and Comparison With Results in References 7 and 8

Dotted line[7]—measured; broken line[8]—theoretical; solid line[7]—theoretical; -.—this work, calculated; (horizontal polarization, λ = 3.2587 cm)

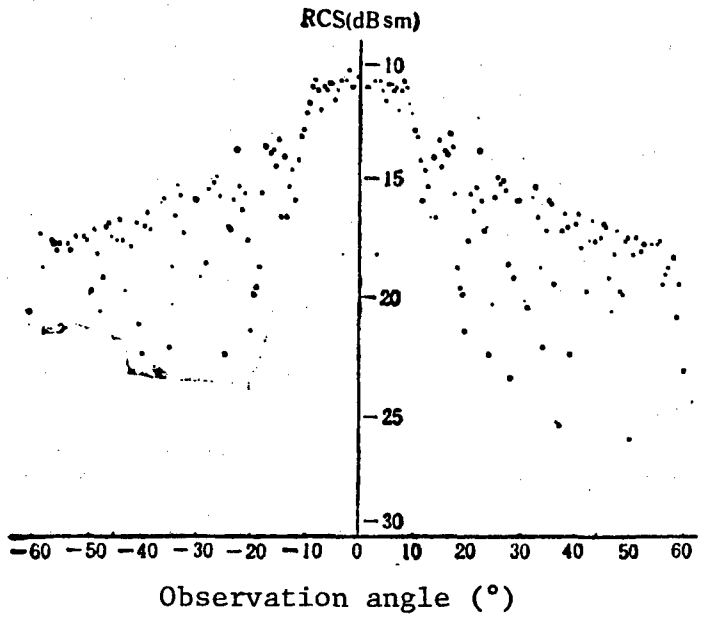

Figure 5. RCS of Model Shown in Figure 3 Under Vertical Polarization

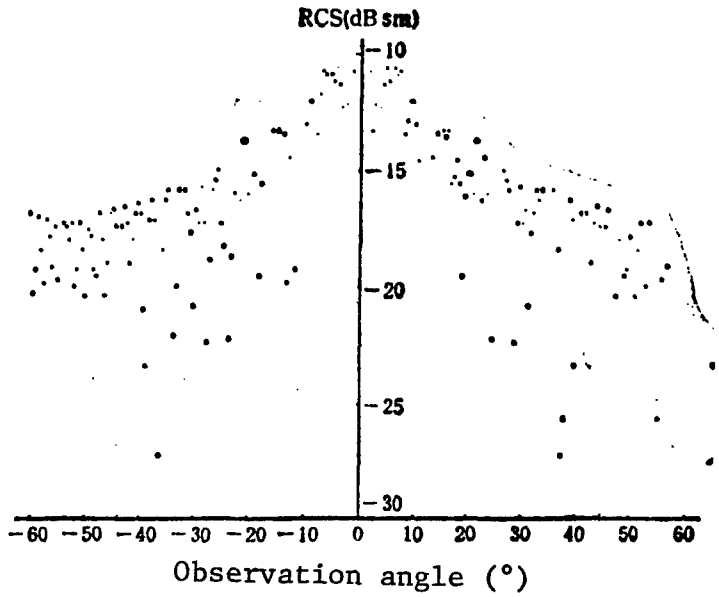

Figure 6. RCS of Model Shown in Figure 3 Under Horizontal Polarization

4. Conclusions

In this work, complex point sources are used to fit a plane-wave field in order to analyze the RCS of a complex target using a near-axis complex-ray approximation method. Based on the example, this method is simple and feasible, and deserving of further investigation and promotion. For example, this method can be used to calculate electromagnetic scattering of complex large-aperture cavities such as a snake-shaped inlet, an intake coated with wave-absorbing material, antenna dome, antenna and radar housing. Relevant results will be published later.

References

1. L. B. Felsen, J. OPT. SOC. AM. A., 3 (1986) 4, 486-496.

2. Ruan Yingzheng, TONGXIN XUEBAO [JOURNAL OF CHINA INSTITUTE OF COMMUNICATIONS], 8 (1987) 4, 49-57.

3. Ruan Yingzheng, CHENGDU DIANXUN GONGCHENG XUEYUAN XUEBAO [JOURNAL OF CHENGDU INSTITUTE OF TELECOMMUNICATIONS ENGINEERING], 16 (1987) 1, 28-33.

4. A. J. Bogush, Jr. and R. E. Elkins, IEEE TRANS. ON AP, AP-34 (1986) 2, 228-243.

5. M. J. Bastiaans, OPTIK, 57 (1980) 1, 95-102.

6. Y. Z. Ruan and L. B. Felsen, J. OPT. SOC. AM. A., 3 (1986) 4, 566-579.

7. H. R. Witt and E. L. Price, PROC. IEE, 115 (1968) 1, 94-100.

8. Guo Rongwei [6753 2837 0251] and Shu Yongze [5289 3057 3419], "Study of Mechanism and Application of Hidden Air Intakes (1)," internal report of Nanjing Institute of Aeronautics, 1987.

Foreign Broadcast Information Service (FBIS) and Joint Publications Research Service (JPRS) publications contain political, military, economic, environmental, and sociological news, commentary, and other information, as well as scientific and technical data and reports. All information has been obtained from foreign radio and television broadcasts, news agency transmissions, newspapers, books, and periodicals. Items generally are processed from the first or best available sources. It should not be inferred that they have been disseminated only in the medium, in the language, or to the area indicated. Items from foreign language sources are translated; those from English-language sources are transcribed. Except for excluding certain diacritics, FBIS renders personal and place-names in accordance with the romanization systems approved for U.S. Government publications by the U.S. Board of Geographic Names.

Headlines, editorial reports, and material enclosed in brackets [ ] are supplied by FBIS/JPRS. Processing indicators such as [Text] or [Excerpts] in the first line of each item indicate how the information was processed from the original. Unfamiliar names rendered phonetically are enclosed in parentheses. Words or names preceded by a question mark and enclosed in parentheses were not clear from the original source but have been supplied as appropriate to the context. Other unattributed parenthetical notes within the body of an item originate with the source. Times within items are as given by the source. Passages in boldface or italics are as published.

SUBSCRIPTION/PROCUREMENT INFORMATION

The FBIS DAILY REPORT contains current news and information and is published Monday through Friday in eight volumes: China, East Europe, Soviet Union, East Asia, Near East & South Asia, Sub-Saharan Africa, Latin America, and West Europe. Supplements to the DAILY REPORTs may also be available periodically and will be distributed to regular DAILY REPORT subscribers. JPRS publications, which include approximately 50 regional, worldwide, and topical reports, generally contain less time-sensitive information and are published periodically.

Current DAILY REPORTs and JPRS publications are listed in *Government Reports Announcements* issued semimonthly by the National Technical Information Service (NTIS), 5285 Port Royal Road, Springfield, Virginia 22161 and the *Monthly Catalog of U.S. Government Publications* issued by the Superintendent of Documents, U.S. Government Printing Office, Washington, D.C. 20402.

The public may subscribe to either hardcover or microfiche versions of the DAILY REPORTs and JPRS publications through NTIS at the above address or by calling (703) 487-4630. Subscription rates will be provided by NTIS upon request. Subscriptions are available outside the United States from NTIS or appointed foreign dealers. New subscribers should expect a 30-day delay in receipt of the first issue.

U.S. Government offices may obtain subscriptions to the DAILY REPORTs or JPRS publications (hardcover or microfiche) at no charge through their sponsoring organizations. For additional information or assistance, call FBIS, (202) 338-6735,or write to P.O. Box 2604, Washington, D.C. 20013. Department of Defense consumers are required to submit requests through appropriate command validation channels to DIA, RTS-2C, Washington, D.C. 20301. (Telephone: (202) 373-3771, Autovon: 243-3771.)

Back issues or single copies of the DAILY REPORTs and JPRS publications are not available. Both the DAILY REPORTs and the JPRS publications are on file for public reference at the Library of Congress and at many Federal Depository Libraries. Reference copies may also be seen at many public and university libraries throughout the United States.